Supporting Information

Eicher et al. 10.1073/pnas.1114944109

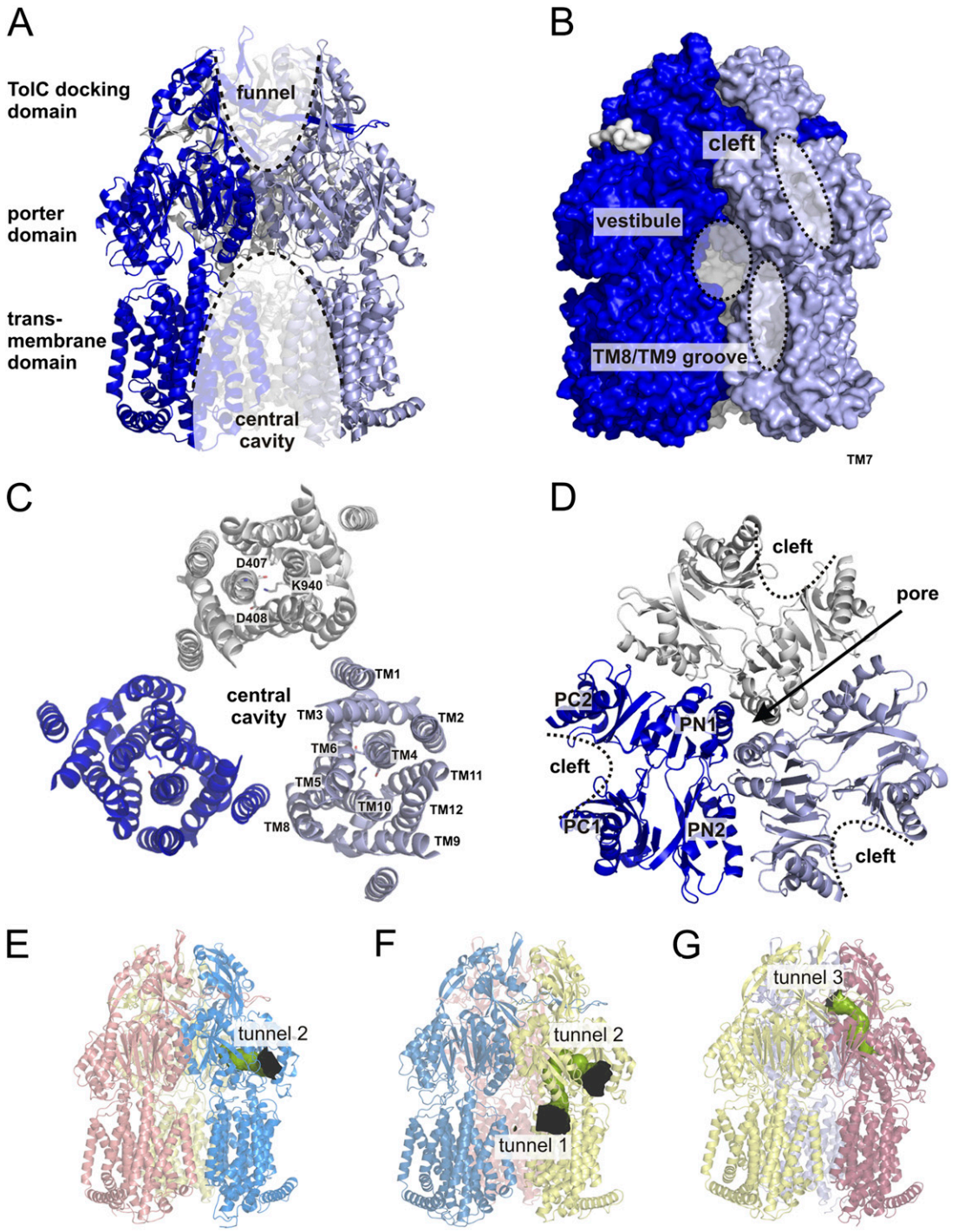

Fig. S1. (*A–D*) Structural features of trimeric AcrB [Protein Data Bank (PDB) ID code: 1IWG]. The monomers are colored in different shades of blue. (*A*) The AcrB trimer (side view, cartoon representation) consists of a transmembrane domain, the periplasmic porter domain, and periplasmic TolC docking domain (as indicated on the left). The central part of the porter domain separates the funnel from the central cavity. (*B*) Side view of the AcrB trimer in surface representation. The central cavity (see *A*) is accessible to solvent via the three vestibules formed in each case at the interface of two monomers. Other potential substrate binding sites (i.e., the PC1/PC2 cleft at the periplasmic porter domain and the transmembrane helix (TM) 8/TM9 groove in the transmembrane domain) are indicated. (*C*) Topological view of the transmembrane domain of trimeric AcrB viewed from the periplasm. Each monomer consists of 12 TMs, with

Legend continued on following page

central TM4 and TM10 harboring three of the four essential charged residues (D407, D408, and K940; not shown is R971 on TM11). The three monomers define the central cavity (see also *A*). (*D*) Periplasmic top view of the AcrB porter domain with subdomains PN1, PN2, PC1, and PC2. The three central α-helices (one from each PN1 subdomain) define a central pore structure (arrow) separating the funnel from the central cavity (as shown in *A*). At the periphery, each monomer harbors a cleft formed at the interface of the PC1 and PC2 subdomains (see also *B*). (*E*–*G*) Visualization of tunnels (in green) in the porter domain of the different monomers (PDB ID code: 2J8S). (*E*) In the loose (L) monomer (blue), tunnel 2 leads from the access site situated in the PC1/PC2 cleft (see *B* and *D*) ≈15 Å above the membrane plane toward the center of the periplasmic porter domain. (*F*) An additional tunnel (tunnel 1) is apparent in the tight (T) conformer (yellow). This tunnel starts at the height of the membrane plane exactly at the periplasmic end of the TM8/TM9 groove (see *B*) and joins tunnel 2 near the deep binding pocket in the T conformer. (*G*) Because of substantial reorientation of the porter subdomains and the coil-to-helix transition at the N-terminal end of TM8, both lateral tunnels collapse in the open (O) conformer (red). Another tunnel (tunnel 3) is created instead and leads from the now-closed deep binding pocket to the funnel in the center of trimer (see *A*).

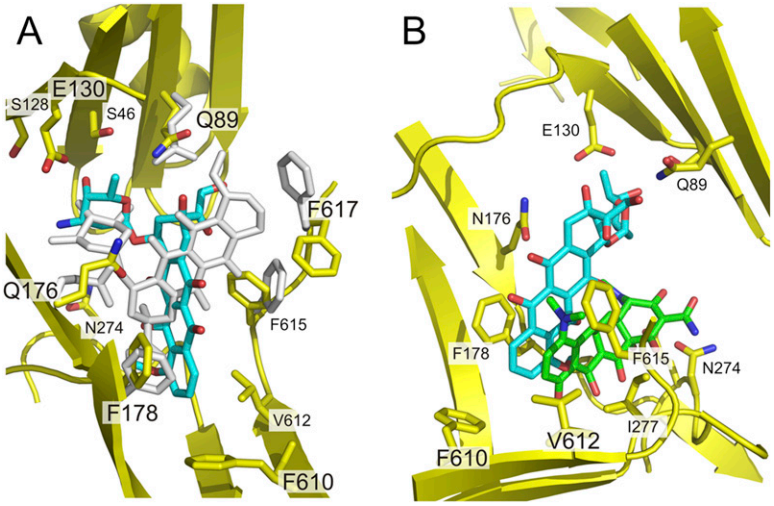

Fig. S2. Superimposition of bound minocycline and doxorubicin in the deep binding pocket of the AcrB T monomer. (*A*) Superimposition of doxorubicin binding in 2DR6 at 3.3-Å resolution (1) and the current structure at 2.25-Å resolution (in yellow, and doxorubicin in cyan; doxorubicin and amino acid side chains of the 2DR6 model that differ substantially are indicated in gray). (*B*) Superimposition of the AcrB cocrystal structures with minocycline (green) and doxorubicin (cyan) in the deep binding pocket of the AcrB T monomer (yellow). The side chains shown here are from the AcrB/minocycline cocrystal structure.

1. Murakami S, Nakashima R, Yamashita E, Matsumoto T, Yamaguchi A (2006) Crystal structures of a multidrug transporter reveal a functionally rotating mechanism. *Nature* 443:173–179.

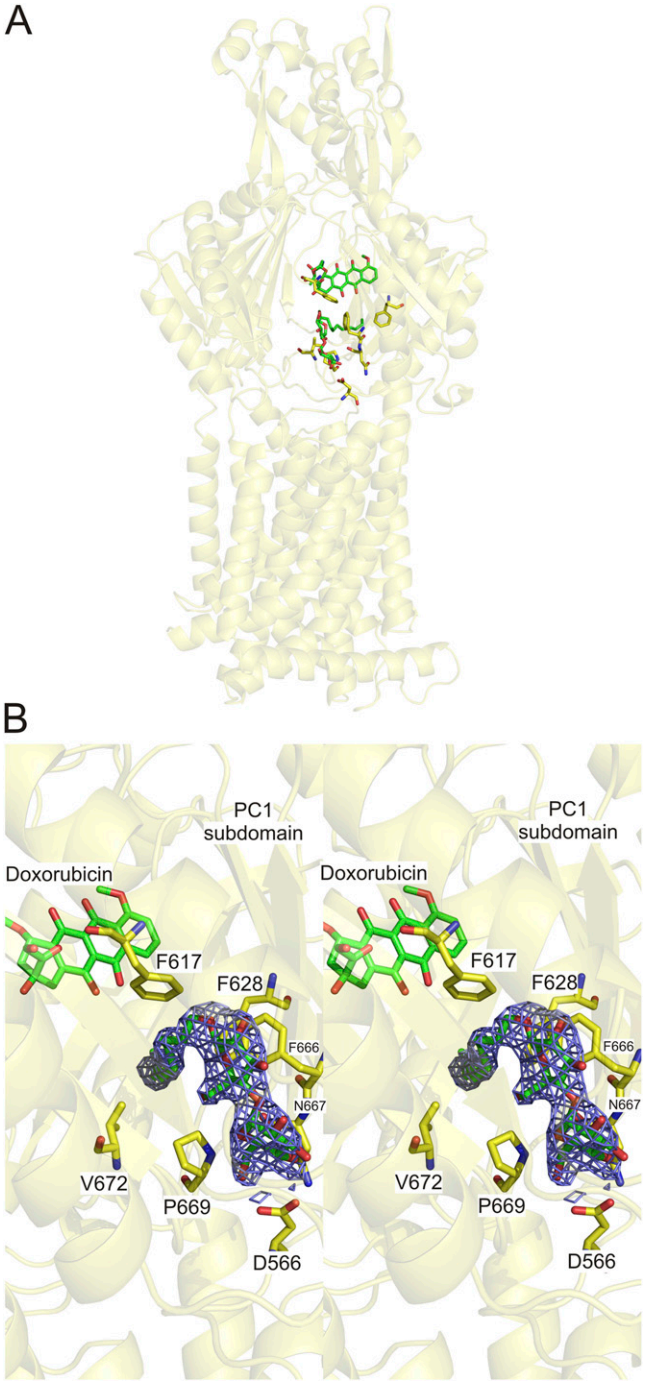

Fig. S3. Binding of doxorubicin in the deep binding pocket and of dodecyl-α-D-maltoside in the lateral binding pocket of the T monomer of the AcrB trimer. (*A*) Side view of the AcrB T monomer parallel to the membrane plane. The view is toward the PC1 and PC2 subdomains. (*B*) Close-up cross-eyed stereo representation of doxorubicin and dodecyl-α-D-maltoside binding. Side-chain interaction (all residues within 3.5-Å distance are shown) with dodecyl-α-D-maltoside is mainly by aromatic stacking interactions (F666) and polar interactions (D566). The blue mesh represents the $2F_o$-F_c electron density map at 1.0 σ.

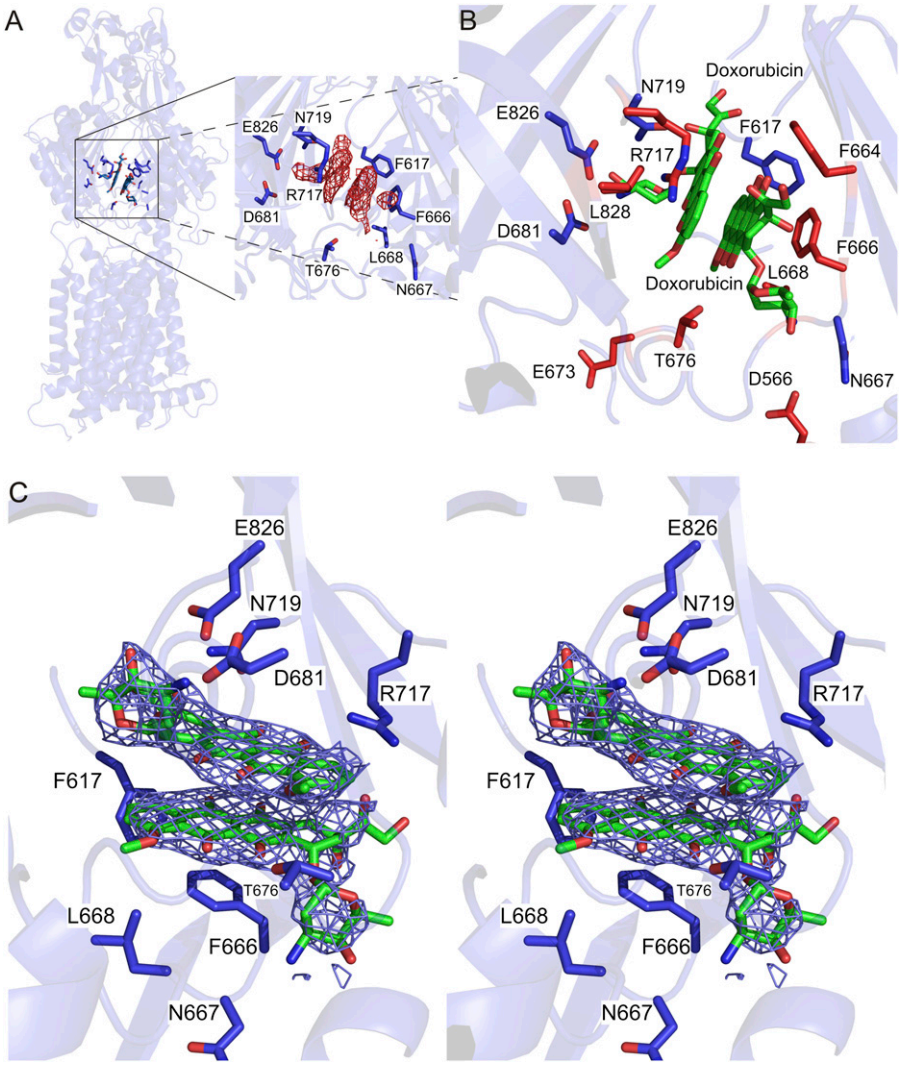

Fig. S4. Binding of doxorubicin in the lateral access pocket of the L monomer. (*A*) Side view of the L monomer in cartoon representation with two doxorubicin molecules bound to the access pocket. *Inset*: Close-up of the access pocket with F_o-F_c densities observed (red mesh) at 3 σ. (*B*) Close-up of the access pocket with two doxorubicin molecules shown in stick representation (green, oxygen atoms in red). Amino acid side chains involved in Bodipy-FL-maleimide labeling after Cys-substitution (1) are shown as red sticks. (*C*) region view as in *B* in cross-eyed stereo representation of the access pocket in the L monomer with two doxorubicin molecules shown in stick representation (green, oxygen atoms in red) and $2F_o$-F_c densities (blue mesh) after refinement at 1 σ. Indicated in *A*–*C* are side chain residues (stick representation, blue, oxygen atoms in red) within 3.5-Å distance of the doxorubicin molecules.

1. Husain F, Nikaido H (2010) Substrate path in the AcrB multidrug efflux pump of *Escherichia coli*. *Mol Microbiol* 78:320–330.

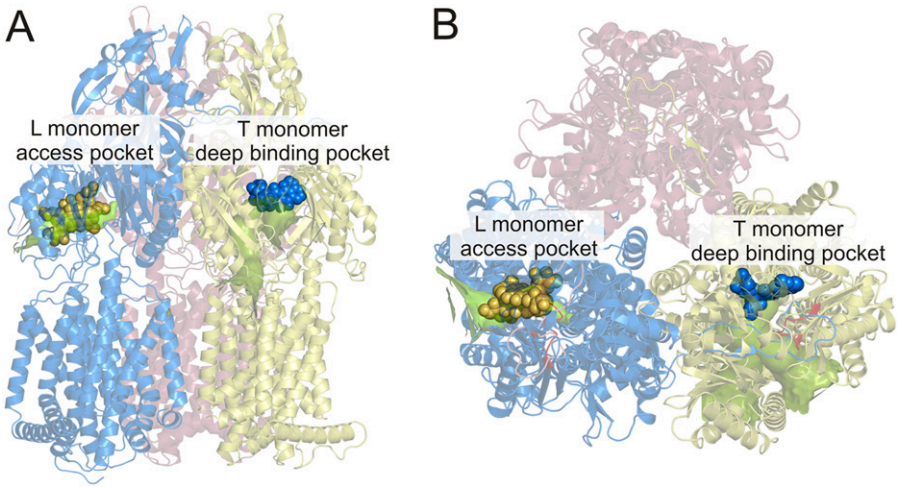

Fig. S5. Localization of the access and deep binding pockets with bound doxorubicin in the asymmetric AcrB trimer. The monomers are colored in blue (L monomer), yellow (T), or red (O). Tunnels (Fig. S1) are visualized in green. (*A*) Cocrystal structure of the asymmetric AcrB trimer (side view, cartoon representation) with two doxorubicin molecules (yellow sphere representation) bound to the access pocket in the L monomer and in the same trimer one doxorubicin (blue spheres) bound at the deep binding pocket in the T monomer. (*B*) Periplasmic top view of the asymmetric AcrB trimer (representation of *A* drawn 90° toward the viewer) with bound doxorubin molecules to the access and deep binding pockets. The switch loops in the L and T monomer are indicated in red.

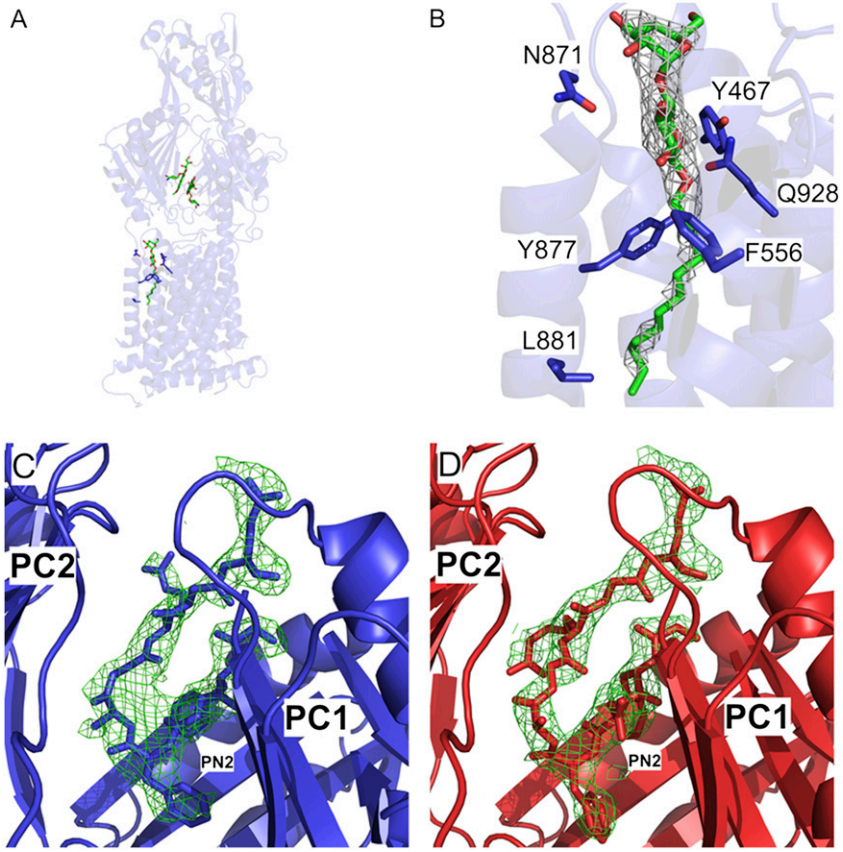

Fig. S6. (*A* and *B*) Binding of dodecyl-β-D-maltoside in the TM8/TM9 groove of the L monomer and proximity to the stacked doxorubicin molecules in the access pocket. (*A*) Side view of the L monomer in cartoon representation (blue). Orientation is identical as in Fig. S4A. Location of the bound dodecyl-β-D-maltoside in the TM8/TM9 region is shown in relation to the bound doxorubicin sandwich in the access pocket of the L monomer. Dodecyl-β-D-maltoside and doxorubicin are presented as sticks (green, oxygen atoms in red). (*B*) Close-up of the TM8/TM9 region. Shown are all side chain residues (stick representation in blue, oxygen atoms in red) within 3.5-Å distance of dodecyl-β-D-maltoside (green stick representation, oxygen atoms in red). Shown in gray mesh is the $2F_o$-F_c density after refinement at 1 σ (2.25-Å resolution). (*C* and *D*) Omit maps for the switch-loop region (amino acid residues 614–622) in the L monomer of (*C*) AcrB/doxorubicin cocrystal structure (blue stick representation) and (*D*) G616N crystal structure (red stick representation). The F_o-F_c densities are indicated in green mesh at 3σ. The presented switch loop regions were built on basis of the F_o-F_c and $2F_o$-F_c densities.

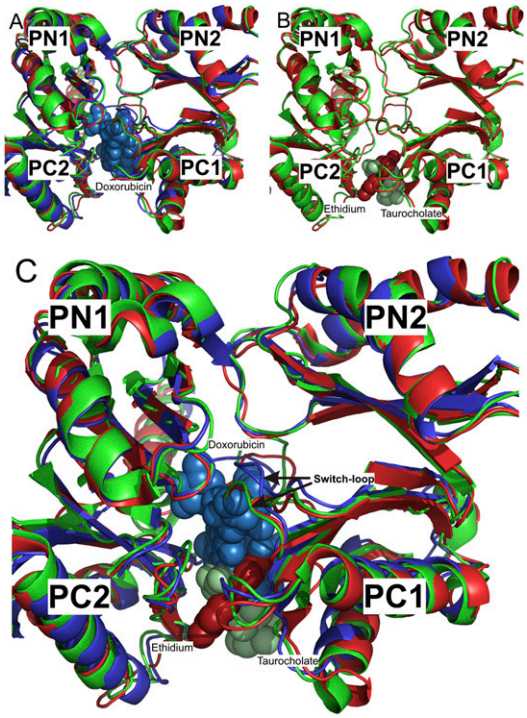

Fig. S7. Binding of ethidium, taurocholate or doxorubicin to the PC1/PC2 cleft. Superimposition of the AcrB porter domain (subdomains PN1, PN2, PC1, and PC2) of monomers derived from the symmetric AcrB structures 1T9X (1) (red, 3.1 Å), 2W1B (2) (green, 3.85 Å) (cocrystal structures with ethidium and taurocholate, respectively) and the L monomer of the asymmetric doxorubicin/AcrB cocrystal structure (blue, 2.25 Å). (*A*) Localization of two doxorubicin molecules (blue sphere representation) in the access pocket of the L monomer of asymmetric AcrB (blue cartoon). (*B*) Localization of ethidium (red spheres) or taurocholate (green spheres) at each of the monomers of symmetric AcrB (PDB ID code 1T9X, red and PDB ID code 2W1B, green) at a more peripheral site in the PC1/PC2 cleft. (*C*) Superimposition of the AcrB porter domain of cocrystal structures 1T9X (with ethidium, red), 2W1B (with taurocholate, green), and the AcrB/doxorubicin cocrystal structure (blue) and localization of ethidium (red spheres), taurocholate (green spheres), and doxorubicin (two molecules, blue spheres) at the PC1/PC2 cleft. The switch-loop positions are indicated by the arrows.

1. Yu EW, Aires JR, McDermott G, Nikaido H (2005) A periplasmic drug-binding site of the AcrB multidrug efflux pump: A crystallographic and site-directed mutagenesis study. *J Bacteriol* 187:6804–6815.
2. Drew D, et al. (2008) The structure of the efflux pump AcrB in complex with bile acid. *Mol Membr Biol* 25:677–682.

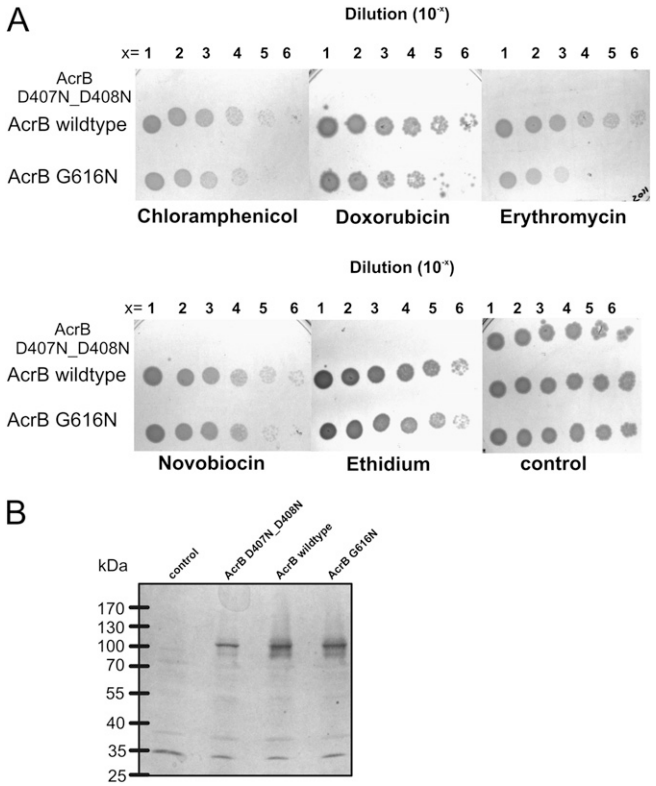

Fig. S8. (*A*) Antibiotic resistance activity of AcrB wild-type, AcrB D407N_D408N, or AcrB G616N in an *E. coli* BW25113ΔacrB background. Growth in the presence of chloramphenicol (1 μg mL^{-1}), doxorubicin (10 μg mL^{-1}), erythromycin (10 μg mL^{-1}), novobiocin (5 μg mL^{-1}), ethidium (50 μg mL^{-1}), and in absence of drug (control) was analyzed on solid LB-agar medium containing 50 μg mL^{-1} kanamycin as selective drug for the pET24 plasmid carrying the AcrB (wild-type or variant) gene. Cells (4 μL of an overnight culture adjusted to an OD_{600} of 1) were diluted as indicated and spotted onto the LB agar plate containing the indicated antibiotics. AcrB D407N_D408N contains substitutions in the putative proton translocation site of AcrB and was previously shown to be devoid of activity for all tested substrates (1). (*B*) Western blot analysis of cell extracts obtained from *E. coli* BW25113Δ*acrB* harboring plasmids encoding wild-type AcrB, G616N variant, D407N_408N variant, or no AcrB (control vector pET24). Cell extracts were obtained from cells growing on solid LB-agar medium as described above, diluted to an OD_{600} of 1.0 in LB medium, and treated as described previously using anti-AcrB rabbit antibodies for immunodetection (1).

1. Seeger MA, et al. (2008) Engineered disulfide bonds support the functional rotation mechanism of multidrug efflux pump AcrB. *Nat Struct Mol Biol* 15:199–205.

Table S1. Data collection and refinement statistics

	wt_mino	wt_doxo	G616N
Data collection and processing			
Space group	$P2_12_12_1$	$P2_12_12_1$	$P2_12_12_1$
Cell dimensions a, b, c (Å)	145.99, 161.74, 246.00	145.94, 163.29, 245.77	145.69, 165.45, 245.42
α, β, γ (°)	90, 90, 90	90, 90, 90	90, 90, 90
Resolution (Å)	39.5–1.9 (2.01–1.90)	49.1–2.25 (2.39–2.25)	50–2.89 (3.07–2.89)
R_{meas}	12.5 (260.2)	10.2 (109.4)	22.9 (159.5)
I/σ_I	12.4 (0.7)	14.9 (1.8)	10.2 (1.4)
Completeness (%)	99.0 (94.2)	99.5 (97.3)	99.7 (98.6)
Multiplicity	6.9 (4.4)	7.0 (5.2)	7.5 (7.4)
Refinement			
Program	Phenix v. dev. 985	Phenix v. dev. 985	Phenix v. dev. 985
Resolution (Å)	39.5–1.90 (1.92–1.90)	49.1–2.25 (2.28–2.25)	49.3–2.9 (2.93–2.90)
No. reflections	450,986	274,555	131,572
R_{work}/R_{free}	20.0/23.1 (43.9/45.9)	18.5/22.7 (31.2/33.9)	21.0/27.1 (33.6/38.1)
No. atoms			
Protein	25,969	25,979	25,987
Ligands and ions	1,258	788	245
	8 LMT (dodecyl-β-D-maltoside)	7 LMT (dodecyl-β-D-maltoside)	7 LMT (dodecyl-β-D-maltoside)
	1 LMU (dodecyl-α-D-maltoside)	1 LMU (dodecyl-α-D-maltoside)	
	26 alkane chains (C14, D12, UND, D10, DD9, OCT, HEX)	3 DM2 (doxorubicin)	
	1 MIY (minocycline)	10 alkane chains (D12, D10, HEX)	
	15 GOL (glycerol)	3 GOL (glycerol)	
	1 SO4 (sulfate ion)		
Water	1,783	1,700	—
B-factors ($Å^2$)			
Average	45.3	51.3	61.8
Protein	44.4	50.4	61.3
Water	45.6	53.0	—
rmsd			
Bond lengths (Å)	0.007	0.007	0.009
Bond angles (°)	1.09	1.05	1.26

Values in parentheses refer to the highest-resolution shell.

Table S2. Distance between deep binding pocket residues and AcrB substrates minocycline and doxorubicin

Doxorubicin (DM2)		Minocycline (MIY)	
Residues	Distance (Å)*	Residues	Distance (Å)*
S46 (CB) - DM2 (O4′)	3.2		
Q89 (NE2) - DM2 (O5′)	3.3		
S128 (OG) - DM2 (O4′)	5.0		
E130 (OE1) - DM2 (C4′)	3.2		
Q176 (OE1) - DM2 (C8)	3.5	Q176 (OE1) - MIY (C71)	5.8
		L177 (O) - MIY (C7)	4.1
F178 (CD1) - DM2 (C20)	3.2	F178 (CE1) - MIY (C71)	3.5
G179 (N) - DM2 (C21)	3.0	G179 (N) - MIY (C16)	3.2
		S180 (CB) - MIY (O7)	3.8
		E273 (OE1) - MIY (C19)	4.0
		N274 (OD1) - MIY (O7)	3.1
I277 (CB) - DM2 (O4)	4.5	I277 (CB) - MIY (O5)	3.0
F610 (CZ) - DM2 (C2)	4.7		
V612 (CG2) - DM2 (C2)	3.8	V612 (CG1) - MIY (C12)	4.1
F615 (CE1) - DM2 (O13)	3.7	F615 (CD1) - MIY (CN7)	3.4

*Shortest interatomic distance.